PATTERN SYNTHESIS FOR EQUAL-GAIN COVERAGE IN AIR-TO-GROUND COMMUNICATION

Le Chang, Yue Li, Zhijun Zhang, and Zhenghe Feng
State Key Lab of Microwave and Communications, Department of Electronic Engineering, Tsinghua University, Beijing, 100084, China; Corresponding author: lyee@tsinghua.edu.cn

Received 29 August 2016

ABSTRACT: *In this article, a new strategy for high-quality and wide-coverage air-to-ground communication is proposed by using pattern synthesis method. The cosecant pattern for equal-gain coverage is synthesized using two switchable patterns, which are provided by switchable feeding networks and a ten-element airborne microstrip antenna array. The merits of the proposed strategy include two folds: first, the antenna array and feeding network are easy to design and with low cost, no need to use beam steering method. Second, the maximum available gain in the required cosecant coverage is achieved by the proposed strategy, providing sufficient path loss margin. We have simulated and fabricated the array prototype, and measured results have proved our idea to achieve equal-gain coverage with a relatively simple antenna structure.*
 Microwave Opt Technol Lett 59:750–753, 2017; View this article online at wileyonlinelibrary.com. DOI 10.1002/mop.30400

Key words: *air-to-ground communication; equal-gain coverage; shaped-beam antenna; maximum available gain*

1. INTRODUCTION

In air-to-ground (AtG) communication, stable and low-noise communication channel is required. Various studies have been reported relating the AtG channels [1–4]. A series of small-scale aeronautical wideband channel models considering the takeoff, taxi, landing, and parking states of an aircraft were proposed for air–ground and air–air links [1]. In Ref. [2], experimental characterization and modelling of the AtG channel over the sea surface with low airborne altitudes was explored. The feasibility of establishing high-quality quantum communication link between a ground station and high-altitude platform was verified using a turboprop aircraft and optical ground station for AtG quantum communication application [3]. The path loss and small-scale fading characteristics of the AtG link which was realized using a quadrocopter and ground station were analyzed and measured [4]. Antenna outfitted with the cosecant pattern plays a vital role in a high-quality channel, and various approaches of the pattern synthesis techniques have been proposed. Reflector and array are two types of antennas used most frequently. By shaping the reflector surface [5–7], using properly designed multiple feeders [8–10] or customizing the reflecting phase of each unit of a planar reflectarray [11–13], any desired patterns can be obtained. The desired pattern may also be achieved by assigning proper excitation amplitude and phase distributions to the array elements [14–17]. Our team also has done some work relating about the beam-shaped array [18–20]. By integrating three leaky-wave coplanar waveguide continuous transverse stub and two 6-stage phase shifters, the main beam can be scanned from 58° to 124° in the E-plane [18]. Using two groups of two-element patch array with different element spacing, two switchable symmetric patterns with flat response were obtained [19]. Using the same synthesis method, six groups of high-gain array with an interleaving architecture were adopted to constitute six-beam switched beam antenna [20]. In the existing array synthesis approaches, the desired patterns are obtained by sacrificing the maximum available gain.

In this article, a new strategy for establishing high-quality and wide-coverage AtG communication channel is proposed using pattern synthesis method. The cosecant pattern required for equal-gain coverage is synthesized by two switchable patterns, which are realized using a ten-element patch array and switchable feeding networks. One of the feeding networks is used to excite all the elements to achieve the maximum available gain, and the other is used to excite part of the elements to produce the radiation pattern which can cover the blind spots left by the former. The resultant communication link provides

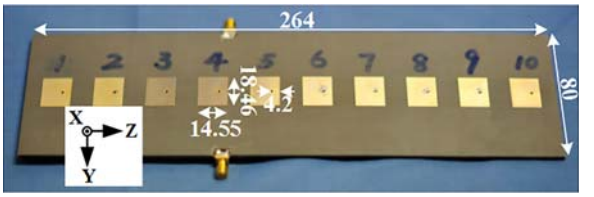

Figure 2 Geometry of the ten-element patch array. [Color figure can be viewed at wileyonlinelibrary.com]

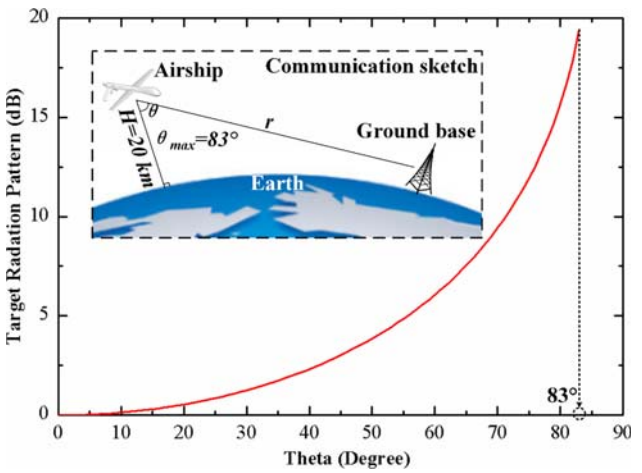

Figure 1 Target radiation pattern (The inset shows the communication sketch). [Color figure can be viewed at wileyonlinelibrary.com]

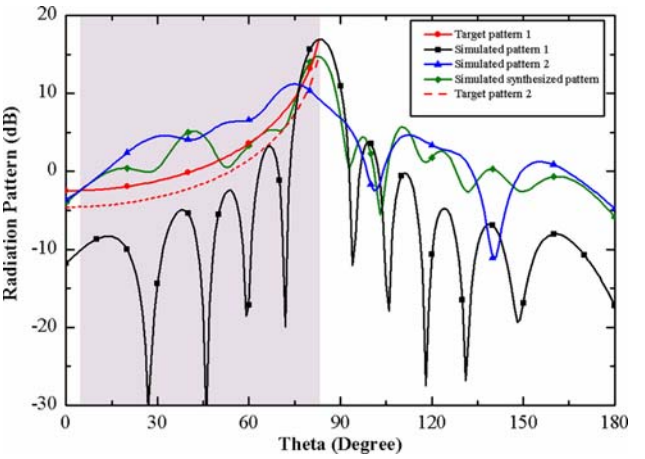

Figure 3 Simulated radiation patterns of the proposed array and synthesized pattern with conventional method. [Color figure can be viewed at wileyonlinelibrary.com]

TABLE 1 Phase Distribution for Radiation Pattern 1

150°	122°	107°	81°	61°	39°	18°	−5°	−25°	−48°

sufficient path loss margin. Most of all, the proposed strategy is easy to design and with low cost, no need to use beam steering.

2. PROBLEM FORMULATION

Here, the application background is put forward as an example: As shown in the inset of Figure 1, when a flying airship communicates with the fixed ground base station, only considering the light of sight (LOS) path, as the airship moves forward, the distance between transmitting and receiving antennas reduces. The normalized target radiation pattern can be obtained through the calculation of the path gain (PG):

$$PG\,(dB) = 20\times\lg\,(r_{nor}) + \mathrm{Gain}_{\mathrm{ref}}$$

$$r_{nor} = r - r_{\min}$$

$$r = (H+R)\times\cos\theta - \sqrt{(H+R)^2\times\cos^2\theta - H^2 - 2\times R\times H}$$

$$r_{\min} = r(\theta = 0^\circ)$$

where H denotes the airship height, R denotes the radius of the earth, and $\mathrm{Gain}_{\mathrm{ref}}$ refers to a constant which is the maximum available gain here. We suppose that the airship is 20 km high and the largest communication angle (θmax) is about 83°. Our target is to achieve a radiation pattern above the target curve for high-quality AtG communication channel with equal-gain coverage, and the objective function is as follows:

$$Pattern\_desired\,(dB) > 20\times\lg\,(r_{nor}) + \mathrm{Gain}_{\mathrm{ref}}$$

3. DESIGN PRINCIPLE

The novel method is verified by using a patch array shown in Figure 2. The proposed array is composed of 10 patches printed on the substrate with a thickness of 1.6 mm, permittivity of 2.55, tangential loss of 0.002, and the inter-element spacing is half of the wavelength in free space. The overall dimensions are 264 mm × 80 mm. The element is a rectangular patch with dimensions of 14.55 mm × 18.46 mm centered at 5.9 GHz and the location of the feeding point is 4.2 mm away from the right edge of the patch.

We used this compact array to produce two radiation patterns: radiation pattern 1 aims to realize the maximum available gain and radiation pattern 2 is used to cover the blind spots left by the former. Figure 3 shows the simulated radiation patterns of the proposed array together with the target curves. The optimization procedure is as follows:

First, radiation pattern 1, aiming to reach the maximum available gain of the array, is obtained with the help of the 10 active radiation patterns;

Second, using a stochastic optimization algorithm, the middle four patches are assigned with the excitation phases and amplitudes ranging from −90° to 90° and 0.5 to 2.5, respectively, aiming to form the radiation pattern 2 which can cover the blind area left by the pattern 1.

TABLE 2 Excitation Coefficients for Radiation Pattern 2

Element	#4	#5	#6	#7
Amplitudes	2	2	1.2	1.2
Phases	89°	2°	−83°	−26°

When all the elements are excited, the excitation amplitudes are equal and the phases shown in Table 1 are the conjugation phases of the active radiation electric fields of the 10 elements at 83° in E-plane. Thus, the radiation patterns of the 10 elements are superimposed with equal amplitude and equal phase at 83° in elevation plane and the corresponding radiation pattern 1 is presented as a black line with a square symbol. As seen, the maximum available gain ($\mathrm{Gain}_{\mathrm{ref}}$) is 16.9 dBi. When the four middle elements are excited with optimal excitation coefficients shown in Table 2 by using a stochastic optimization algorithm and others are connected to a match load, the radiation pattern 2 is presented as a blue line with a triangle symbol. The crossover point of the two patterns is about 77°. The two simulated patterns above the target pattern range from 77° to 83°, and from 5° to 77° in elevation plane, respectively. When the airship reaches this angle, a handover between two radiation patterns is required. The maximum gain is 16.9 dB which is the maximum available gain of the proposed array. There is a blind spot below the angle 5°, but this area is not a concern because communication is not needed at a distance of this close between the airship and the ground. Thus, a communication link is formed from 5° to 83° as indicated by the gray section.

TABLE 3 Optimal Phases for Conventional Shaped-Beam Method

137°	87°	78°	−2°	−23°	−68°	9°	−68°	−140°	−46°

For comparison, a radiation pattern with good performance using the conventional shaped-beam method is given in Figure 3 as green line with a rhombus symbol. The optimal phases obtained by a stochastic optimization algorithm are shown in Table 3. The maximum gain of the conventional shaped-beam array is 14.8 dB at 83° and the pattern can ensure communication of the same angle range as well as the proposed method by sacrificing the gain of 2.1 dB (comparing the target curve 1 to the target curve 2). At low elevation angle, the path-loss margin is not sufficient, resulting in the pattern being sensitive to phase fluctuation and the bumpiness of the airship. A large path-loss margin is achieved by sacrificing the maximum available gain, so the maximum available gain and a sufficient path-loss margin cannot be able to acquire simultaneously.

The proposed method has overcome the disadvantages of the conventional beam shaping method. On one hand, the proposed array can achieve the maximum available gain as aforementioned. On the other hand, as can be seen, the pattern 2 is much higher than the target curve 1, it means the proposed method preserves a larger path-loss margin at the lower elevation angle, thus it allows sever bumpiness during the flight.

4. FEEDING NETWORKS

The feeding networks designed using the software Advanced Design System (ADS) 2009 adopt parallel-fed structures. Detailed description of the feeding networks is given in Figure 4(a). The output amplitudes are achieved by quarter-wavelength impedance transformers and the phase distribution is controlled by adjusting the transmission line length between the input and output ports. "TL1" to "TL7" present impedance transformers whose characteristic impedances are 71, 77, 55, 57, 49, 47, and 41 Ω, respectively. The rest of the transmission lines are delay

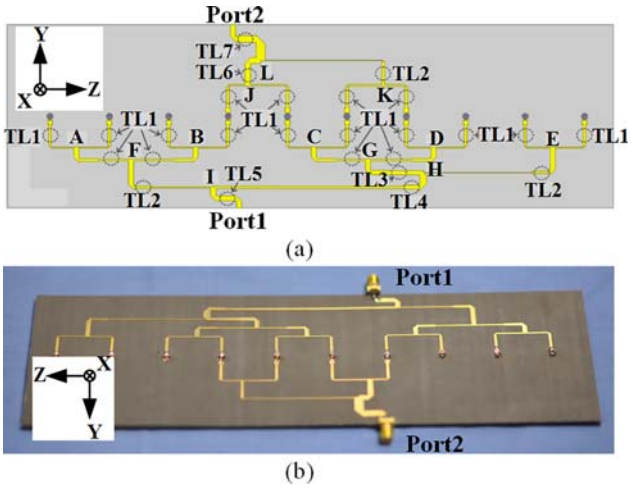

Figure 4 (a) Description of the feed networks, and (b) Prototype of the feed networks. [Color figure can be viewed at wileyonlinelibrary.com]

lines and the phase requirements are controlled by adjusting the locations of point "A" to "I", and point "J" to "L", respectively. The fabricated prototype is shown in Figure 4(b). Finally, the antenna consists of two layers: The top one with the proposed array and the lower one with the two feeding networks; the ground plane lies between two substrates. When feeding the port 1, 10 bond wires are used to connect the outputs of the network 1 to the 10 patches; when feeding the port 2, the former 10 wires are removed and another four bond wires are adopted to connect the outputs of the network 2 to the middle four patches.

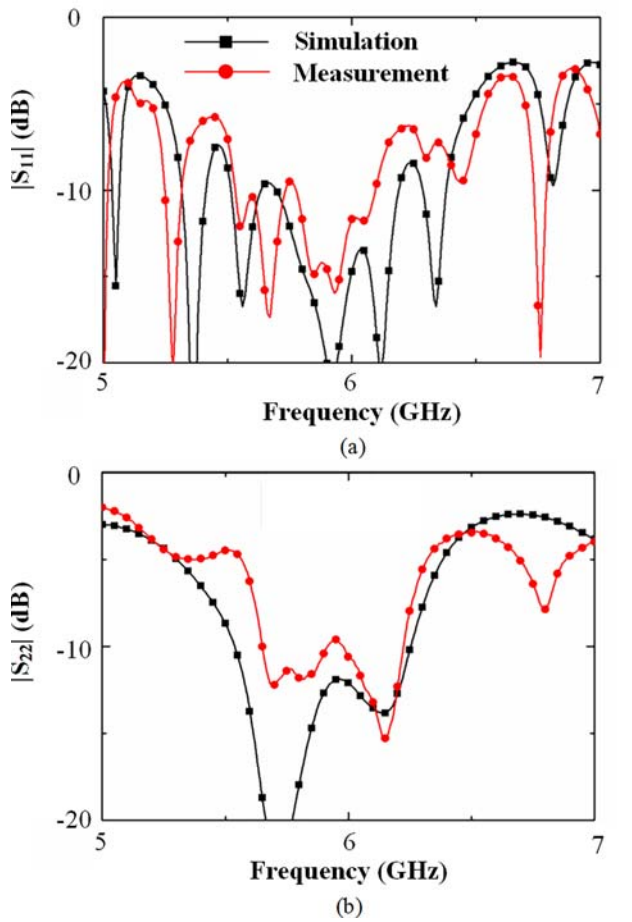

Figure 5 Simulated and measured reflection coefficients from (a) port 1, and (b) port 2. [Color figure can be viewed at wileyonlinelibrary.com]

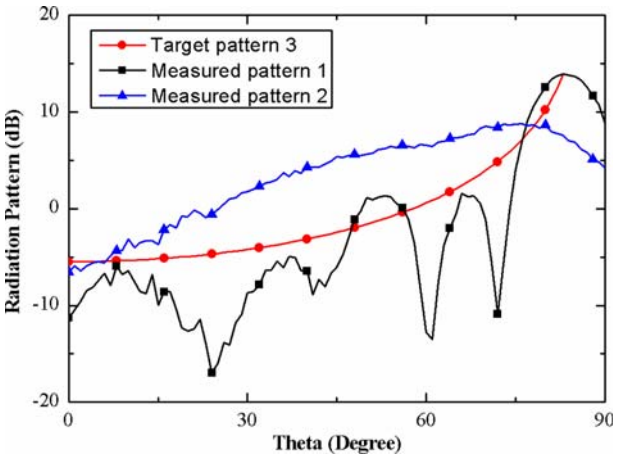

Figure 6 Measured radiation patterns. [Color figure can be viewed at wileyonlinelibrary.com]

5. MEASUREMENT RESULT

The simulated and measured reflection coefficients from the two ports are shown in Figure 5. The measured reflection coefficients from both ports are in good agreements with the computed results. The simulated reflection coefficients of the two ports have −10 dB impedance bandwidths of 500 MHz (5.68–6.18 GHz) and 710 MHz (5.54–6.25 GHz), respectively, whereas the measured results are 360 MHz (5.73–6.09 GHz) and 570 MHz (5.65–6.22 GHz), respectively. There are many messy resonance points out of band from port 1: they are caused by the match effect of the network.

The measured radiation patterns from the two ports are shown in lines with rhombus symbol and triangle symbol in Figure 6. The maximum gain is 14 dB, which is 2.3 dB lower than the simulation result. This is caused by Ohmic and dielectric losses of the array and feed lines and the effect of tolerances in fabrication and measurement errors. The two patterns above the target pattern ranges from 5° to 83° in elevation plane and the crossover point is 77°. This agrees well with the simulation. Thus, a communication link is formed from 5° to 83°.

Therefore, the merits of the proposed strategy include two folds: first, the antenna array and feeding network are easy to design and with low cost, no need to use beam steering method. Second, the maximum available gain in the required cosine coverage is achieved by the proposed strategy, providing sufficient path loss margin.

6. CONCLUSION

In this article, a simple strategy for establishing high-quality and wide-coverage AtG communication channel is presented using pattern synthesis method. A low-cost ten-element patch array fed using two switchable feeding networks is fabricated to verify the strategy. Combining the two patterns provided by two feeding networks, the maximum available gain and wide equal-gain coverage are achieved.

ACKNOWLEDGMENT

This work was supported by the National Natural Science Foundation of China under Contract 61301001 and the China Postdoctoral Science Foundation funded project 2015T80084.

REFERENCES

1. E. Haas, Aeronautical channel modelling, IEEE Trans Veh Technol 51 (2002), 254–264.
2. Y. Meng, and Y. Lee, Measurements and characteristics of air-to-ground channel over sea surface at C-band with low airborne altitude, IEEE Trans Veh Technol 60 (2011), 1943–1948.
3. S. Nauerth, F. Moll, M. Rau, C. Fuchs, J. Horwath, S. Frick, and H. Weinfurter. Air-to-ground quantum communication, Nat Photon 7 (2013), 387–393.
4. E. Yanmaz, R. Kuschnig, and C. Bettstetter, Achieving air–ground communication in 802.11 networks with three-dimensional aerial mobility, in Proceedings IEEE INFOCOM, 2013, pp. 120–124.
5. T. Katagi, and Y. Takeichi, Shaped-beam horn-reflector antennas, IEEE Trans Antennas Propag 23 (1975), 757–763.
6. S. Karimkashi, A. Mallahzadeh, and J. Rashed-Mohassel, A new shaped reflector antenna for wide beam radiation patterns, in Proceedings of International Symposium on MAPE, Hangzhou, China, 2007, pp. 535–538.
7. M. Mahajan, R. Jyoti, K. Sood, and S. Sharma, A method of generating simultaneous contoured and pencil beams from single shaped reflector antenna, IEEE Trans Antennas Propag 61 (2013), 5297–5301. Oct.
8. M. Milijic, A. Nesic, and B. Milovanovic, Design, realization, and measurements of a corner reflector printed antenna array with cosecant squared-shaped beam pattern,"IEEE Antennas Wireless Propag Lett 15 (2016), 421–424.
9. A. Foudazi, and A.R. Mallahzadeh, Pattern synthesis for multi-feed reflector antenna using invasive weed optimization, IET Microwave, Antennas Propag 6 (2012), 1583–1589.
10. A.D. Monk, P.J.B. Clarricoats, and Z. Hai, An array-fed mesh reflector for multiple spot beam and reconfigurable shaped beam operation, IEE Colloquium on Hybrid Antennas, London, May 1993.
11. D. Pozar, S. Targonski, and R. Pokuls, A shaped-beam microstrip patch reflectarray, IEEE Trans Antennas Propag 47 (1999), 1167–1173.
12. J. Zornoza, R. Leberer, J. Encinar, and W. Menzel, Folded multilayer microstrip reflectarray with shaped pattern, IEEE Trans Antennas Propag 54 (2006), 510–518. Feb.
13. E. Carrasco, M. Arrebola, J. Encinar, and M. Barba, Demonstration of a shaped beam reflectarray using aperture-coupled delay lines for LMDS central station antenna, IEEE Trans Antennas Propag 56 (2008), 3103–3111. Oct.
14. N. Herscovici, Nonplanar microstrip arrays, IEEE Trans Antennas Propag 44 (1996), 389–392.
15. L. Freytag, and B. Jecko, Cosecant-squared pattern antenna for base station at 40 GHz, APS , (2004) 2464–2467.
16. M. Chang, and W. Weng, Synthesis of cosecant array factor pattern using particle swarm optimization, in Proceedings of the International Symposium on Antennas Propagation, Nanjing, October 2013, pp. 948–951.
17. M. He, Z. Hao, and K. Fan, A planar millimeter wave antenna with a cosecant squared pattern, in APMC, Najing, 2015.
18. Y. Li, M. Iskander, Z. Zhang, and Z. Feng, A new low cost leaky wave coplanar waveguide continuous transverse stub antenna array using metamaterial-based phase shifters for beam steering, IEEE Trans Antennas Propag 61 (2013), 3511–3518.
19. H. Wang, Z. Zhang, and Z. Feng, A beam-switching antenna array with shaped radiation patterns, IEEE Antennas Wireless Propag Lett 11 (2012), 818–821.
20. H. Wang, Z. Zhang, Z. Feng, and M. Iskander, A switched beam antenna with shaped radiation pattern and interleaving array architecture," IEEE Trans Antennas Propag 63 (2015), 2914–2921.

MULTIBAND OMNIDIRECTIONAL PLANAR MONOPOLE ANTENNA WITH TWO SPLIT RING RESONATOR PAIRS

Dang Oh Kim,[1] Che-Young Kim,[2] Dae-Geun Yang,[2] and Mohammad Sajjad Ahmad[2]

[1] 1st Research Division Team 2, Poongsan Defense R&D Institute, 266 Techno 2-Ro Yuseong-Gu, Daejeon 34027, South Korea

[2] School of the Electronics Engineering, Kyungpook National University, 80 Daehakro Bukgu, Daegu 41566, South Korea; Corresponding author: cykim@ee.knu.ac.kr

Received 4 September 2016

ABSTRACT: *This letter presents a printed planar monopole antenna with triple-band operation. By adding two symmetrical split ring resonator (SRR) pairs to the primitive monopole antenna, the wireless local area network (WLAN), and worldwide interoperability for microwave access (WiMAX) bands operating at 2.45/3.5/5.8 GHz can be obtained. The inserted SRR pairs exhibit both the radiation and the nonradiation mode of operations, from which the proposed antenna works in triple band. The principle of how these two modes give us the multiband operation is explained. The antenna was fabricated and measured to confirm the characteristics of the proposed design. The simulated and experimental results are in close agreement.* © 2017 Wiley Periodicals, Inc. Microwave Opt Technol Lett 59:753–758, 2017; View this article online at wileyonlinelibrary.com. DOI 10.1002/mop.30390

Key words: *multiband antenna; split ring resonator; planar monopole; omnidirection; wireless local area network*

1. INTRODUCTION

Recently, the demand for antennas with multiband characteristics, compact size, appropriate impedance bandwidth, and omnidirectional radiation pattern has increased rapidly. These devices allow innovation to wireless data communication device manufacturing industries, that is, in smart phones, tablet PCs, and so forth. The antennas used in these portable devices are typically based on the planar monopole antenna. To obtain multiband characteristics, various types of planar monopole antennas have been proposed [1–5]. In particular, triple-band planar monopole antennas using split ring resonators (SRRs), which is the most common metamaterial resonator shape, are proposed in [6,7]. Gemio proposed the triple-band planar monopole antenna by adding an SRR around the monopole antenna [6]. In 2011, Ntaikos suggested that multiband antenna operation can be achieved by inserting the SRR into the folded monopole antenna [7]. In these studies, three operating bands are achieved by applying the SRR to the planar monopole antenna. The triple-band antenna proposed in [6] does not possess the characteristics of two independent bands. The antenna reported in [7] achieves the two additional resonant bands with a single band monopole antenna by employing the mutual coupling between a SRR and a monopole antenna. Consequently, these antennas have the drawback of being difficult to control in terms of their respective operating bands. Our proposed design overcomes this shortcoming. The triple-band antenna allows independent control of the operation of the monopole antenna and the two SRR pairs.

In general, the aim of a transmitting antenna is to radiate the maximum energy into the space. By contrast, the SRR operates as a nonradiating element for certain modes, holding its nonradiating reactive energy within a limited space. This relationship has been loosely addressed in the aforementioned studies of monopole antennas [6,7]. The details of the radiation quality factor of the electrically small antennas given were very brief.